An L-Band Study of Cascade Range Volcanoes, Global Persistently Active Volcanoes, and Areas of Active Deformation within the Western USA

PI Number 059
Charles W. Wicks[(1)]
Zhong Lu[(2)]

[(1)] U. S. Geological Survey, 345 Middlefield Rd, MS 977, Menlo Park, Calif. USA 94025, Phone: 650-329-4874, FAX: 650-329-5163, E-mail: cwicks@usgs.gov
[(2)] U.S. Geological Survey, Cascades Volcano Observatory, 1300 SE Cardinal Court, Building 10, Suite 100 Vancouver, WA 98683 , E-mail:zlu@usgs.gov

1. INTRODUCTION

The PALSAR data has proven essential in conducting deformation studies in areas of heavy vegetation. There are two areas that we summarize below: 1) Chaitén volcano in Chile's Southern Andean Volcanic Zone, and 2) The Sulu Volcanic Center in Papua New Guinea. In each case the only useful geodetic measurements available were in the form of interferograms calculated from ALOS PALSAR data.

2. CHAITÉN VOLCANO

The most viscous liquid magma is rhyolite, so it was surprising that on May 2, 2008 Chaitén Volcano, located in Chile's southern Andean volcanic zone (SAVZ), viscous magma migrated from greater than 5 km depth in less than four hours and erupted explosively with only two days of precursory seismic activity. The last major rhyolite eruption previous to Chaitén was the largest volcanic eruption in the 20th century – it occurred at Novarupta volcano, Alaska, in 1912. Because of the explosive nature of rhyolite eruptions and because of the surprisingly short warning before the eruption at Chaitén volcano any information about the workings of the magmatic system at Chaitén, and rhyolitic systems in general, is important from both the scientific and hazards perspectives. Here we present surface deformation data related to the Chaitén eruption based on radar interferometry observations from the Japan Aerospace Exploration Agency (JAXA) DAICHI (ALOS) satellite. The data, the first for an explosive rhyolite eruption, indicate the rapid ascent of rhyolite occurred via diking and that melt segregation and magma storage were controlled by existing faults**.**

Chaitén volcano is situated on a forearc sliver between the Chile-Peru subduction zone and the Liquiñe-Ofqui fault zone (LOFZ), Fig. 1. The LOFZ is a long-lived shear zone that has accommodated transpressional (northward translational and eastward compressional) movement of

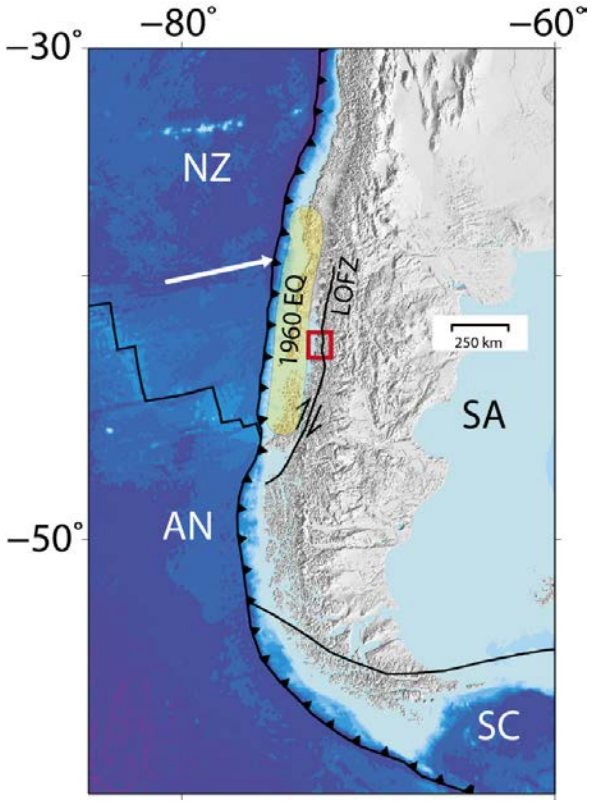

Fig. 1. Chaitén key map. Tectonic plates are Nazca (NZ), South American (SA), Scotia (SC) and Antarctic (AN). The Nazca Plate converges on the South American plate at a rate of about 68 mm/yr as shown by the white arrow. The approximate rupture area of the Mw 9.5 1960 earthquake is labeled. The detailed study area shown in Fig. 2 is shown with the red box. The Liquiñe-Ofqui Fault Zone (labeled LOFZ) is a major transpressional fault zone that cuts through the study area.

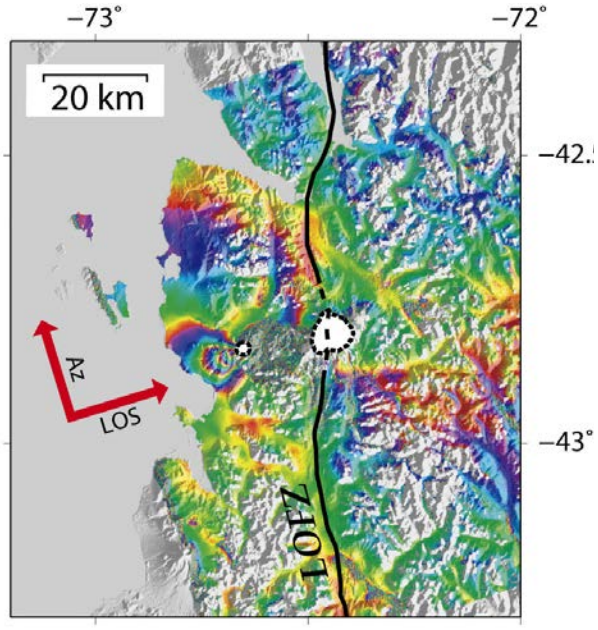

Fig. 2 An interferogram from ascending orbits 09599 (acquired on 2007/11/13) and 21677 (acquired on 2010/02/18) with a perpendicular baseline of 130 m. The direction of the satellite's orbit is shown with the red arrow labeled "Az" in each panel. The line-of-sight look direction from the satellite to the ground is shown with the red arrow labeled "LOS". The black line labeled LOFZ marks the approximate location of the main strand of the Liquiñe-Ofqui Fault Zone. The dashed black lines mark the approximate location of the Michimahuida Pleistocene collapse caldera (after ref 5-REF_KILIAN) and smaller Chaitén caldera, on the west. The incidence angle for each interferogram is ~39° from vertical. Over 40 cm of movement on the west side of Chaitén volcano is directed away from the satellite.

the forearc sliver for at least the last ~4 Ma. Chaitén has a ~3 km diameter caldera that is part of the Michimahuida-Chaitén volcanic complex (Fig. 2). The dacitic to basaltic Michimahuida volcano, located in the LOFZ ~15 km east of Chaitén, has a larger ~8 km diameter caldera that formed in the Pleistocene and was subsequently filled by dacite and later basalt effusion.

Although the study area is heavily vegetated and the time intervals between acquisitions are long, the 23.6 cm wavelength of the radar instrument enabled us to calculate useful interferograms (Figs. 2,3 & 4). In 2010 JAXA acquired descending mode radar data, enabling the calculation of descending mode interferograms--the most coherent one is shown in Fig. 4. Together the two ascending mode interferograms in Figs. 2&3 span the time interval covered by the descending mode interferogram shown in Fig. 4. The descending mode interferogram displays a broad area of movement (~50 cm maximum) away from the satellite that encompasses the entire Michimahuida-Chaitén volcanic complex – it is absent in

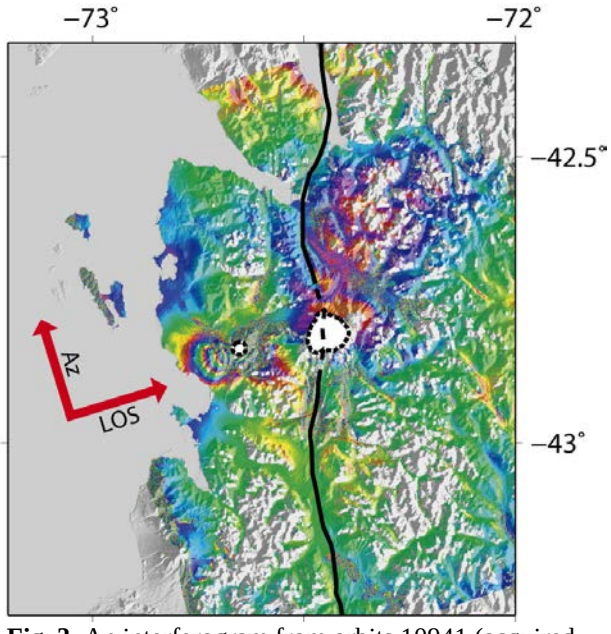

Fig. 3 An interferogram from orbits 10941 (acquired on 2008/02/13) and 23019 (acquired on 2010/05/21) with a perpendicular baseline of 404 m. It shows the same deformation pattern seen in Fig. 2. We were able to calculate ascending mode interferograms months after the 2008 eruption that displayed the same deformation field shown in Figs. 2 & 3. A narrow lath-shaped contracting dike, from the surface to ~10km depth, that trends to the NW is all that is required to fit this signal.

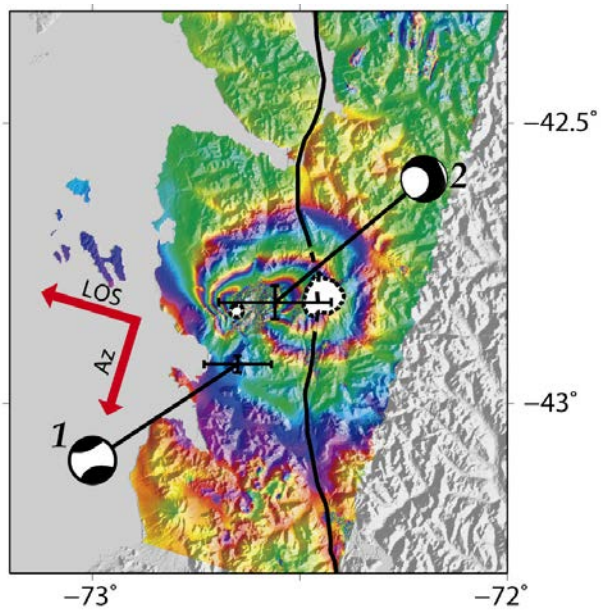

Fig. 4 An interferogram calculated from two descending radar scenes from orbits 09868 (acquired on 2007/12/01) and 21946 (acquired on 2010/03/08) with a perpendicular baseline of 41 m. The two CMTs are plotted with the estimated two standard deviation error bars (www.globalcmt.org).

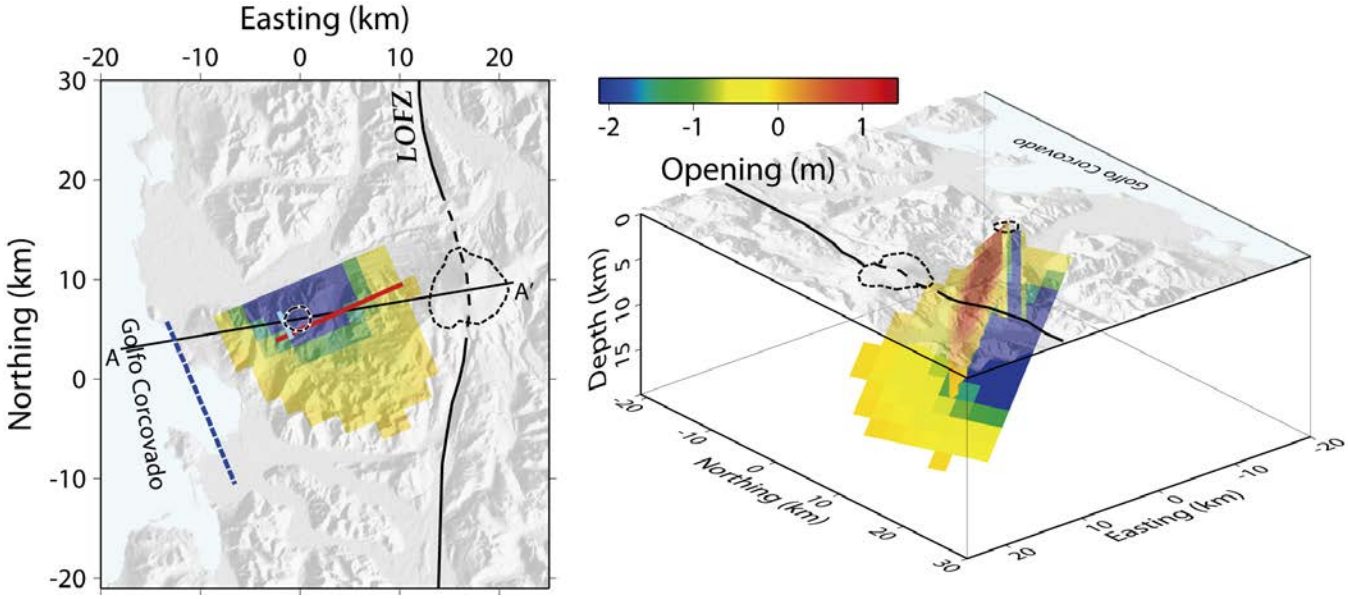

Fig. 5 The model is composed of three planar bodies of distributed plane perpendicular opening or closing: one deep collapsing body that dips to the ENE, one vertical dike that opens progressively as it shallows under Chaitén to the west, and one vertical lath like body of collapse that intersects both the deep dipping collapse body and the dike and it essentially reaches the surface at Chaitén Volcano. The outline of Michimahuida and Chaitén calderas and the approximate location of the LOFZ are shown. **left**, plan view of the best-fit model where the peak collapse in the deep body is constrained to 2 m. The surface trace of the dike is red and the surface trace of the lath-shaped body is cyan. The plane containing the deep collapse body is projected to reach the surface at the dashed blue line. It dips about 40° to the ENE and is about 10 km deep below Chaitén. The black line through the two calderas shows the location of cross-section A-A' in Fig. 6. **right**, a perspective of the model viewed from the NE

the ascending mode interferograms. The radar beams from both modes of acquisition intersect the Earth's surface at an angle of about 39° from vertical. In the descending mode the satellite looks to the WNW whereas in the ascending mode it looks to the ENE (red arrows in Fig. 2-4). Consideration of the radar geometry yields two important points: 1) the deformation source responsible for the broad deformation signal is not a volumetric source, and 2) it should be a sill-like collapsing source that dips to the ENE with a dip angle that is approximately complementary to the radar incidence angle.

Under the assumption of an Earth model that is a uniform homogeneous elastic half-space, we determined that three separate deforming bodies are required to fit the data: 1) a collapsing sill-like body that dips to the ENE, 2) a near vertical expanding dike that trends to the ENE and extends from the deeper collapse body to the surface at Chaitén volcano, and 3) a collapsing vertically dipping lath-shaped body that surfaces near the west rim of Chaitén caldera (Fig. 5). Models consisting of only two deforming bodies yielded a significantly worse fit. We also modeled the data with a dike and a listric fault that incorporated the two collapsing bodies, but the fit to the data was significantly worse than the best-fit models. So, the overshoot of the large ENE dipping body up-dip from the vertical lath-shaped body is a required feature. The dip of the deep collapse body is between 24 and 54° to the ENE and the depth of the body directly below Chaitén volcano is between 8 and 12 km. The maximum amount of collapse on the deep collapse body is not well determined, but can be roughly bounded. In Fig. 5 we show one viable model with variable distribution of collapse on the deep body. The model shown in Fig. 5 is the result of constraining the maximum collapse to be 2 m whereas the an equally viable model (not shown) is the result of constraining the maximum collapse to be 8 m. The fit to the data is nearly identical for each model and for all intervening values of maximum collapse with a variance for the residual of ~3 cm^2 for each model and each model accounting for ~98% of the data variance. The two models represent loose bounds on a family of best fit models with maximum collapse between 2 and 8m on the deep collapse body --the variance of the misfit increases for models constrained to have maximum collapse less than 2 m and greater than 8 m on the deep collapse body. As of about March 2010, the net volume decrease represented by the three sources in the model is 150-250 million m^3. The estimated volume of material erupted during the May 2008 Plinian eruption, plus the new dome is about 700-900 million m^3. This relationship between change in reservoir volume compared to erupted volume is an expected consequence of magma compressibility and not necessarily an indication of magma recharge.

Because of a lack of nearby seismic instrumentation, earthquake locations during the beginning phases of the eruption are not useful for additional constraints on the deformation sources. However, Centroid Moment Tensor (CMT) solutions, recorded for the largest earthquakes, are consistent with our model. Only two shallow earthquakes in the study area were large enough for CMT solutions to be calculated at the Global CMT Project (www.globalcmt.org) (Fig. 4). CMT #1 (Fig. 4) is the solution for a Mw 5.2 earthquake that occurred about two hours before the main explosive event at 08:00 UTC on May 2, 2008. CMT #2 (Fig. 4) is the solution for a Mw 5.0 earthquake that occurred about 20 hours after the onset of the main explosive event. CMT #1 is consistent with a near vertical dike that trends to the ENE, the same as our modeled dike (Fig 6b). CMT #2 is consistent with a collapsing sill-like body that dips ~42° to the ENE, the same as our modeled deep sill-like body (Fig. 6c). As noted by Lohman et al. [1], seismic data can be used to determine an accurate earthquake mechanism, but without instrumentation close to the source, accurate earthquake locations cannot be determined. The location and depth of CMT solutions have been shown to be biased by tens of kms in remote locations [2]. In Fig. 6 we plot the projected CMT mechanisms with the realization that depths are likely biased.

The nature of the inferred faults in Figs. 5&6, west of the LOFZ, is consistent with recent studies, that outlined pop-up structures at latitudes immediately south of the Michimahuida-Chaitén volcanic complex. The pop-up structures are defined by a structural high centered on the LOFZ, that is bounded on the west by east dipping reverse faults and on the east by west dipping reverse faults that merge at depth with the LOFZ. Shear structures sub-parallel to the main LOFZ shear are found between the reverse faults. We interpret the dipping sill-like collapse body to be a reservoir of rhyolitic magma that occupies an ENE dipping reverse fault that is part of a pop-up structure centered on the LOFZ. The rhyolite reservoir appears to tap a zoned magma body under Michimahuida that is the site of basaltic influx. The reverse fault is an effective path for magma migration and segregation of low density melt.

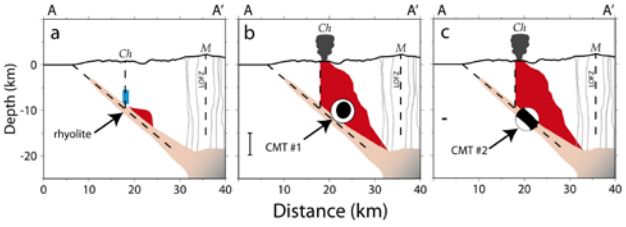

Fig. 6 Schematic interpretation of the involvement of deformation sources in the May 2, 2008 eruption of Chaitén. The location of cross-section A-A' is shown in Fig. 5, the position of Chaitén (Ch) and Michimahuida (M) volcanoes are labeled on the elevation profile. The dashed black lines show the approximate location of the LOFZ and inferred fault splays. The salmon colored area is the rhyolite reservoir that grades into a zoned magma chamber beneath Michimahuida. **a**, The seismicity, beginning on April 30, 2008 indicates initiation of diking (colored red) into rock above an inflated dipping sill**. b**, Continued diking leads to the injection earthquake (projection of CMT #1) just over two hours before the explosive eruption. The dike impinges upon a vertical strand of the LOFZ beneath Chaitén, the location of the collapsing lath-like body**. c**, On May 3, nearly 19 hours after the eruption began, the dipping sill collapses catastrophically (projection of CMT #2) after a critical amount of magma has been withdrawn.

2. SULU VOLCANIC CENTER

Interferograms from two paths (357 and 358 in Figure 1) were used to investigate an especially energetic earthquake crisis that occurred in July of 2006. The crisis led to the evacuation of several villages, because of fears of an imminent eruption. Although the crisis occurred early in the ALOS mission there were three pre-crisis acquisitions and one post-crisis acquisition on path 357 and one pre-crisis and one post-crisis acquisition on path 358.

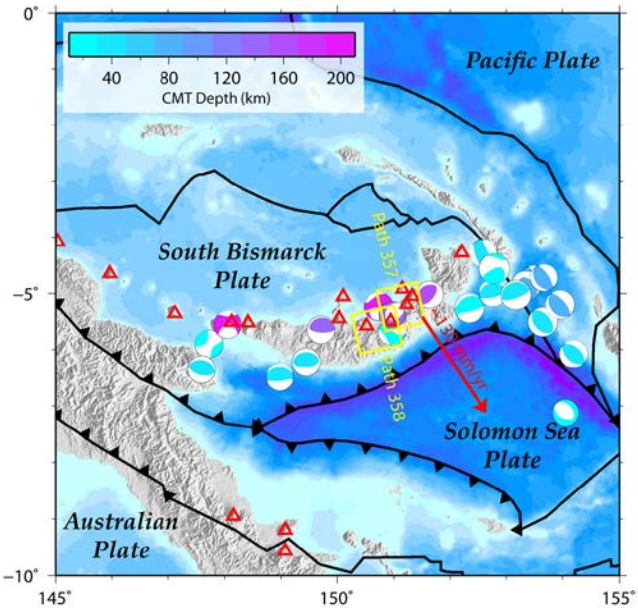

Fig. 7. Tectonic setting of New Britain Island (center of image). Moment tensors of all earthquakes Mw 7 and greater, since 1976 in the global centroid moment tensor(CMT) catalog (www.globalcmt.org) are shown, color coded to depth. Active volcanoes are marked with red triangles. The Solomon Sea Plate subducts beneath the South Bismarck Plate at about 130 mm/yr. The two scenes used are shown with the yellow squares (paths as labeled).

Below, we show one pre-crisis interferogram and two co-crisis interferograms that captured the deformation field related to the seismic crisis. The baselines for the two co-crisis interferograms were large (over 2 km) but the flat lying areas were still mostly coherent. The baseline for the one pre-crisis interferogram was 130 m and the whole

scene, even the steep densely forested highland, was coherent. We processed the data with GAMMA, using a high resolution one second SRTM DEM.

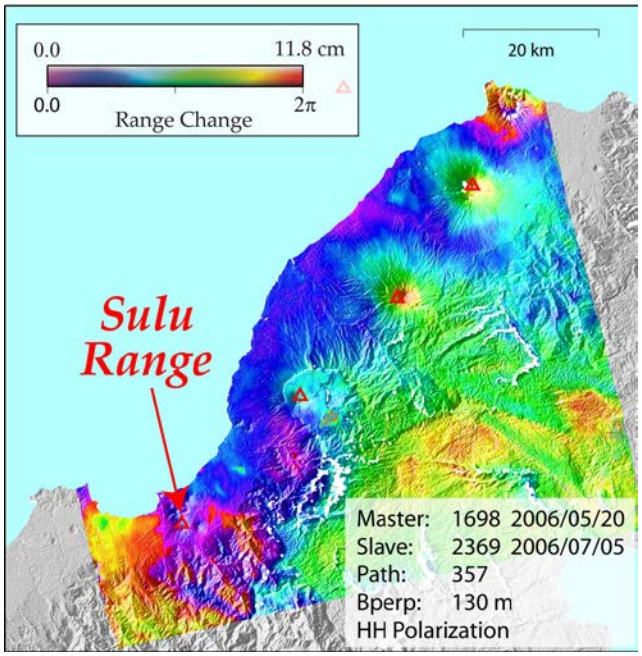

Fig. 8. This is the one pre-crisis interferogram -- it also has the best baseline. The red triangles mark the locations of the active volcanoes. The colorscale maps color into range change and it applies to all interferograms shown. The Sulu Range is the location of the July 2006 seismic crisis.

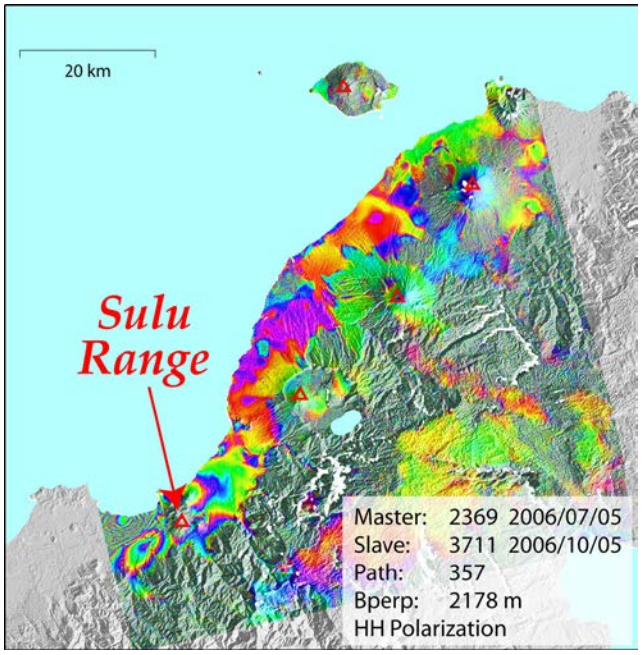

Fig. 9. A three month interferogram on PATH 357 covering the July 2006 Sulu seismic crisis in the extreme near range. Much of the deformation along the coast is probably related to changing water levels in coastal swamps.

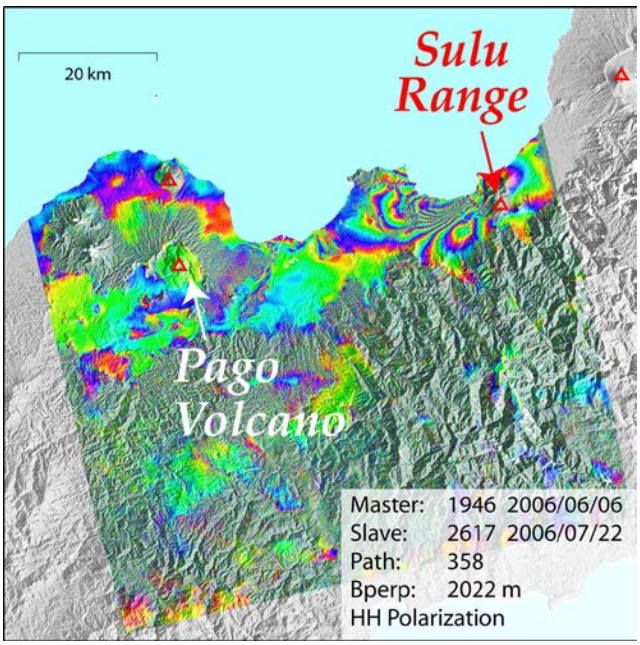

Fig. 10. Co-crisis interferogram for PATH 358. The deformation near the Sulu Range is apparent and signal related to lava emplacement from the 2003 Pago eruption

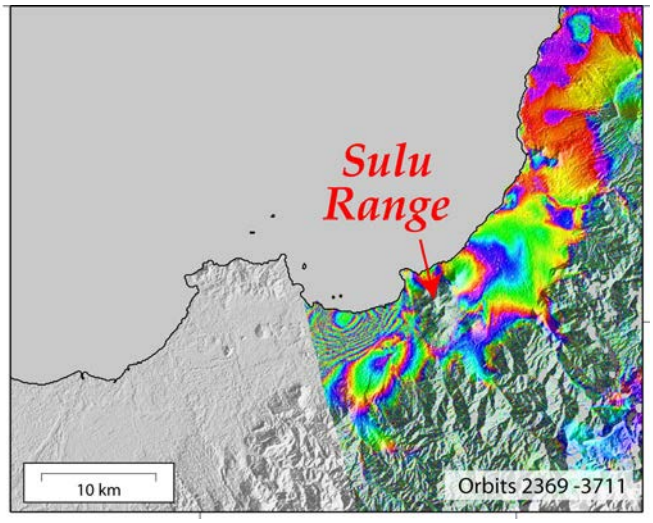

Fig. 11. A high resolution interferogram from Path 357 showing the deformation associated with the July2006 Sulu seismic crisis.

The two co-crisis interferograms (shown in high resolution in Figs. 11 and 12) show over 1 meter of peak to peak deformation -- over 0.8 meters of positive range change (movement away from the satellite) and over 0.2 meters of negative range change (movement toward the satellite).

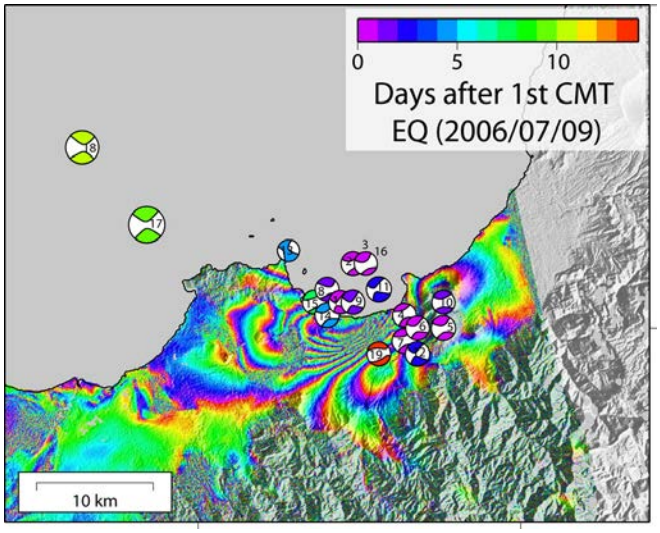

Fig. 12. A high resolution interferogram from Path 358 showing the deformation associated with the seismic crisis. Nineteen of the earthquakes during the crisis were large enough for CMT solutions (shown) to be determined (www.globalcmt.org). The color of the mechanism shows the time (in days) after the first earthquake (July 9, 2006) with a CMT solution. The numbers correspond to the earthquakes listed in Table 1.

Table 1. CMTs from large earthquakes during seismic crisis shown in Figs. 8 and 9.

CMT No.	Date	Depth	Mw
1	2006/07/09	17.97	4.8
2	2006/07/09	13.35	4.8
3	2006/07/09	16.36	4.8
4	2006/07/09	12.00	4.8
5	2006/07/10	16.83	5.0
6	2006/07/10	13.45	4.9
7	2006/07/10	12.00	5.1
8	2006/07/11	20.88	4.9
9	2006/07/11	15.40	4.9
10	2006/07/11	19.90	4.8
11	2006/07/11	12.00	5.1
12	2006/07/12	12.00	5.0
13	2006/07/13	14.36	5.2
14	2006/07/14	13.10	5.0
15	2006/07/16	12.00	4.8
16	2006/07/17	12.00	4.8
17	2006/07/19	15.00	6.4
18	2006/07/19	15.39	5.9
19	2006/07/23	12.00	4.9

The deformation data from the interferograms are not sufficient to uniquely constrain a source of deformation, however, the CMT mechanisms are consistent with a dike intrusion (or dike intrusions). Prior to modeling, the data from paths 357 and 358 were parsed using a quadtree method. Efforts fitting the data with only a dike do not fit the data sufficiently. A normal fault is required above the dike, to accommodate the affect of dike opening on the overlying shallow crust. In figure 9, we show the best-fit model that was found using a nonlinear method that combines a Monte Carlo and gradient method. The top of the dike is at a depth of 10 km, opens about 8 m (uniformly) with a volume of about 0.6 km^3 of magma. The normal fault is about 2.8 km deep with about 4.2 m of slip.

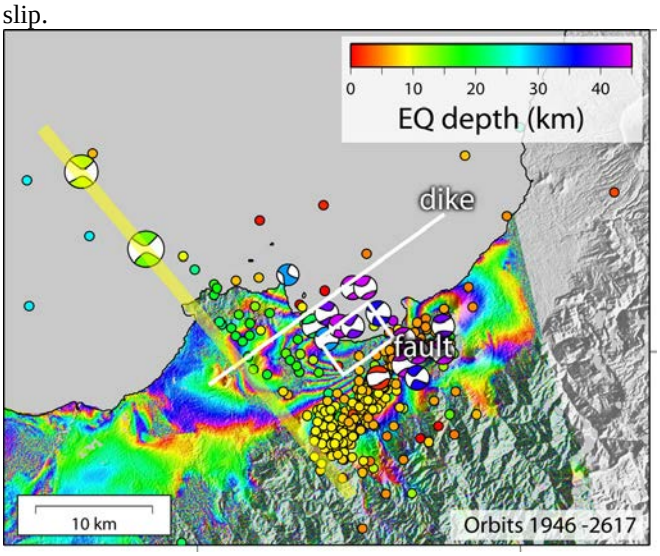

Fig. 13. The best-fit dike and fault model (white lines show the surface projections, as labeled). The same CMT solutions as shown in Figure 8 (Table 1) are shown. Aftershock data (black circles filled with color) were recorded by Geoscience Australia and the personnel at Rabaul Volcanological Observatory beginning July 21, 2006, for 17 days. The fill color of the earthquake symbol indicates the earthquake depth, as shown by the color scale. The broad yellow line is an interpreted strike-slip fault that probably represents the termination of dike intrusion.

In our interpretation dike intrusion began near or under the Sulu range and propagated southwest until the rupture of the earthquakes on July 19 (Mw 6.4 and 5.9) which terminated the intrusion. The Yellow line in Figure 9 shows the possible termination fault lines up with the two large July 19 earthquakes, a lineation in the aftershock seismicity, and a disturbance in the path 358 interferogram.

6. REFERENCES

[1 Lohman, R. B., Simons, M. & Savage, B. Location and mechanism of the Little Skull Mountain earthquake as constrained by satellite radar interferometry and seismic waveform modeling. J. Geophys. Res. 107, doi:10.1029/2001JB000627 (2002).

[2] Lohman, R. B. & Simons, M. Locations of selected small earthquakes in the Zagros mountains. Geochem. Geophys. & Geosyst. 6, doi:10.1029/2004GC000849 (2005).